

# Combining Density-Functional Theory with Low-Temperature, Polarized Terahertz Spectroscopy of Single Crystals Explicates the Fundamental Modes of L-Alanine

J. L. Allen, T. J. Sanders, J. Horvat, and R. A. Lewis  
*Institute for Superconducting and Electronic Materials and School of Physics,  
University of Wollongong, Wollongong, NSW 2522, Australia.\**

K. C. Rule  
*Australian Centre for Neutron Scattering, Australian Nuclear Science  
and Technology Organisation, Lucas Heights, NSW 2234, Australia*

(Dated: November 30, 2022)

Density-functional theory may be used to predict both the frequency and the dipole moment of the fundamental oscillations of molecular crystals. Suitably polarized photons at those frequencies excite such oscillations. Thus, in principle, terahertz spectroscopy may confirm the calculated fundamental modes of amino acids. However, reports to date have multiple shortcomings: (a) material of uncertain purity and morphology and diluted in a binder material is employed; (b) consequently, vibrations along all crystal axes are excited simultaneously; (c) data is restricted to room temperature, where resonances are broad and the background dominant; (d) comparison with theory has been unsatisfactory (in part because the theory assumes zero temperature). Here, we overcome all four obstacles, in reporting detailed low-temperature polarized THz spectra of single-crystal L-alanine, assigning vibrational modes using density-functional theory, and comparing the calculated dipole moment vector direction to the electric field polarization of the measured spectra. Our direct and detailed comparison of theory with experiment corrects previous mode assignments for L-alanine, and reveals unreported modes, previously obscured by closely-spaced spectral absorptions. The fundamental modes are thereby determined.

Alanine ( $C_3H_7NO_2$ ) is an amino acid which is naturally occurring in the human body. It is the simplest amino acid to demonstrate chirality. Alanine was one of the earliest amino acids, fundamental to early life for metabolic processes and protein formation [2, 3]. In modern life, alanine is essential to many peptide and protein structures, whose hydrogen bonds and van der Waals interactions mediate essential biochemical functions. Recently, the simplest amino acid, glycine, has been found to form in interstellar space through a non-energetic mechanism, and it is suspected that the next-simplest amino acid, alanine, may also [4]. L-Alanine forms a molecular crystal. Each molecule is in a zwitterionic form, where the amine and carboxylic groups are ionized. As is evident in the molecular crystal structure shown in Fig. 1(a), this charge distribution gives rise to a dense and complex network of hydrogen bonds [1].

Low-energy hydrogen bonds, such as those which constitute crystalline L-alanine, are associated in energy with electromagnetic radiation in the terahertz (THz) region. For this reason, terahertz spectroscopy has served as an effective probe of the intermolecular interactions of a wide range of biomolecules [5–10] and pharmaceuticals [11, 12] and is an appropriate technique to characterize the interactions in L-alanine. Terahertz spectroscopy has been used to assign vibrational modes, elucidate the mechanics of protein formation and function [13], and unravel molecular dynamics [14]. More generally, terahertz physics is an emerging field of wide application [15]. The terahertz roadmap [16] predicts numerous advances, which have recently spanned terahertz axions [17], meta-

materials [18], and field-induced ferroelectricity [19].

Returning now to molecular crystals, the precise origins of the terahertz modes are poorly understood. They are usually inferred from the mode energy and crystal structure. In contrast to the bulk of experimental data reported, which does not use polarized radiation, polarized (‘anisotropic’) THz spectroscopy distinguishes vibrational modes with respect to crystal symmetry via the orientation of the dipole moments [20]. This technique also permits the observation of modes that would otherwise be obscured by closely spaced absorption bands [21, 22]. Thus, polarized THz spectroscopy allows for a much more precise mode assignment, yielding better insight into the physical origin of the observed modes.

We now focus on alanine. While it has been intensely studied in the low-energy spectral region [7, 10, 23–32], many questions relating to its molecular dynamics are still to be answered with precision, due to inadequate theory and experiment. This is due to five main factors.

First, density-functional theory (DFT) calculations, while prolific [9, 33–36], in many cases only agree poorly with experimental spectra. The difficulty may be often traced to the use of functionals that do not model intermolecular hydrogen bonds well. As mentioned above, such bonds are largely responsible for the low-energy vibrational modes in alanine. This issue has only recently been identified [37] and will be fully resolved here.

Secondly, the precise characterization of L-alanine in the terahertz region is hampered by the lack of high-quality samples. Previous studies have commonly used blends containing L-alanine in a binding medium for pel-

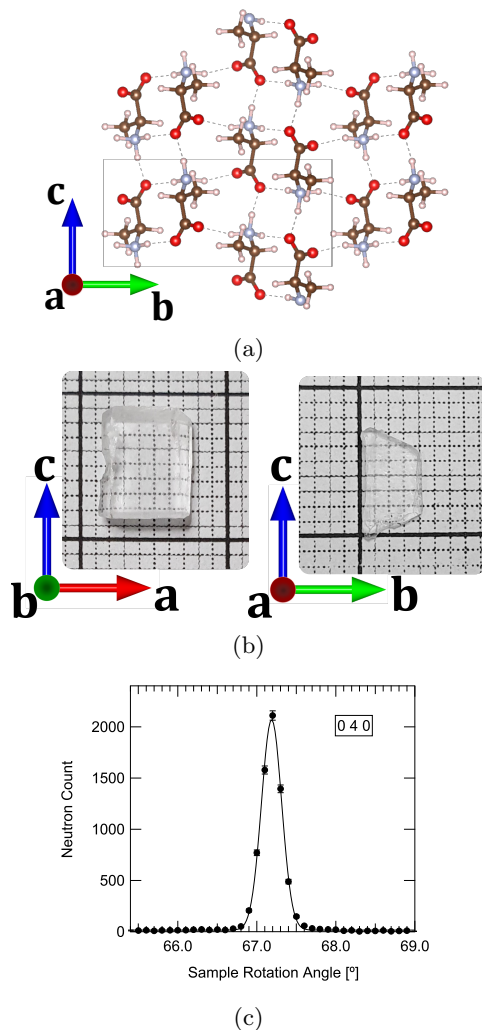


FIG. 1: (a)  $1.5 \times 2$  unit cells of L-alanine. Dashed lines denote hydrogen bonds (with the threshold set to  $2.10 \text{ \AA}$ ). The box represents one unit cell. Structure from Lehmann *et al.* [1]. (b) L-alanine single crystals. On the left is the crystal with *c*-axis vertical and *a*-axis horizontal, used for *a*-axis and *c*-axis polarized synchrotron spectra. On the right is the crystal with *c*-axis vertical and *b*-axis horizontal, used for *b*-axis polarized synchrotron spectra. Both are shown on a 1 cm-grid. (c) The 040 reflection of a single crystal of L-alanine measured with  $2.345 \text{ \AA}$  neutrons at ANSTO using the Taipan thermal triple-axis spectrometer. The solid line is a Gaussian fit to the data. The narrow reflection peak width indicates a high degree of monocrystallinity.

lets [9, 25, 27]. The single-crystal approach of this work removes the potential of observing extrinsic features arising from the binder or interactions between the binding media and the material under study. Moreover, single crystals scatter less light than pellets.

Thirdly, the use of crystals permits the modes associated with different crystallographic axes to be excited by linearly polarized radiation. Polarized THz spectroscopy provides direct information to compare to DFT modeling concerning the dipole moment direction.

Fourthly, the polarized data allows us to separate modes which were previously obscured.

Fifthly, by measuring at low temperatures, where resonances are sharper, we have been able to observe previously unidentified modes with unparalleled clarity.

We now outline our theoretical approach. Further details are provided in the Supplemental Material. [38] DFT was used to calculate the vibrational modes in L-alanine. The CRYSTAL17 package was used [39]. Initial atomic coordinates from Lehmann *et al.* [1] were the seed for full geometric optimization of both atomic positions and the unit cell.

Zwitterionic amino-acids have proven very difficult to model with DFT methods to the accuracy required for obtaining THz spectra comparable to experiment. Key to our modeling is the choice of an appropriate DFT functional. The B97-3c functional was chosen on three grounds: it includes an appropriate basis set, is fast and accurate in modeling non-covalent interactions that are important for this crystal. The B97-3c functional has been successful in modeling other molecular crystals [40–42]. It uses van der Waals interactions, and short-range basis set corrections. Modified def2-TZVP basis sets [43] are used, specifically mTZVP [43, 44]. The B97-3c functional is a low-cost Generalized Gradient Approximation (GGA) functional 2–3 times faster than the standard GGA functional when used with the mTZVP basis set. Even though faster, it has been shown to perform with an accuracy level better than the standard GGA functionals for light, main group elements [40].

Since accurate modeling of the experimental terahertz spectrum of L-alanine has proved to be difficult [9, 33, 45], very tight convergence criteria were employed for the full geometry optimization. The details are given in the Supplemental Material [38]. The infrared absorption spectrum was calculated in the harmonic approximation for the final converged geometry. The intensities of the absorptions were calculated with the Berry phase approach [46, 47].

We now characterize the samples. Single crystals were grown using the solvent evaporation method [48]. The crystals used for measurements are shown in Fig. 1(b). Two crystals were used, one with an *a*-face and one with a *b*-face, to allow all three principal crystallographic axes to be probed. For optimum anisotropic measurements, it is best to ensure that only one crystallographic axis is probed in any one measurement. Ideally the sample should be monocrystalline. The morphology of the samples was determined using elastic neutron scattering on the Taipan thermal triple-axis spectrometer [49] at the Australian Nuclear Science and Technology Organ-

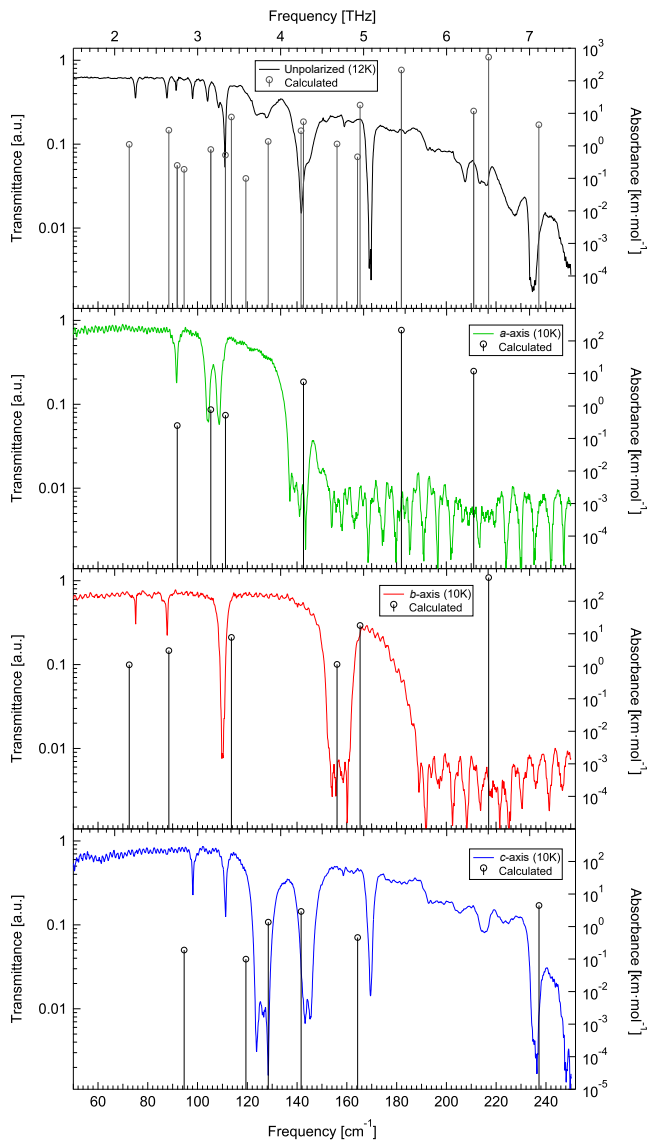


FIG. 2: Polarized THz measurements at 10 K along each crystallographic axis of L-alanine compared to DFT calculation mode positions for the  $a$ -axis,  $b$ -axis, and  $c$ -axis, as well as the unpolarized spectrum at 12 K.

isation (ANSTO), and agrees with the accepted growth morphology [50]. In checking the orientation, the 040 reflection peaks in the L-alanine single crystals were found to have a low mosaic spread, of  $\sim 0.8^\circ$ , as may be seen in the sample rotation scan in Fig. 1(c). This is (only just) larger than the instrumental resolution of  $0.66^\circ$ . Figure 1(c) also indicates a good fit of the data to a Gaussian curve, which is expected for a crystalline reflection peak; moreover, there are no obvious additional peaks. This is also true for  $\theta$ - $2\theta$  scans performed on the crystal samples. The same holds for the scans done on the 120 reflection peak (as seen in Supplemental Fig. S3 [38]). The good Gaussian fits and the relatively narrow mosaic spreads suggests the samples are highly crystalline, and confirms

that they are suitable for polarization measurements.

We now present our results. Anisotropic THz spectra of L-alanine were measured using synchrotron radiation at the Australian Synchrotron. The light was polarized using a rotatable wire-grid polarizer. The polarized experimental transmittance spectra of L-alanine are shown in Fig. 2. The  $a$ -axis and  $c$ -axis spectra were measured with the sample having the face perpendicular to the  $b$ -axis (left-hand sample in Fig. 1(b)). The  $b$ -axis spectrum was measured on the sample having the face perpendicular to the  $a$ -axis (right-hand sample in Fig. 1(b)). The frequency positions and absorbance intensities from our L-alanine DFT calculations are also shown on the same plots for electric dipoles excited by crystalline vibrations along the direction of the each of the three axes.

The polarized spectra of L-alanine coincide well with the unpolarized spectrum (Fig. 2; also Fig. S4 and the discussion in Supplemental Material [38]). All features seen in the unpolarized spectrum appear distinctly in one of the polarized spectra. Furthermore, calculated modes from DFT also align well with the experimental spectra in Fig. 2, with the the same number and approximately equivalent positions of the calculated modes and experimental absorption bands. Additionally, Fig. 3 shows the evolution of absorption bands as the incident polarization angle is varied. All absorption features fade systematically as the electric field polarization is rotated away from the axis along which the absorption is associated.

With the incident electric field of the THz radiation polarized in the  $a$ -direction, absorption bands are observed at 2.74, 3.12, and 3.26 THz, with a broad absorption band at 4.25 THz, which is not completely resolved as it reaches the noise floor. These experimental results are in good agreement with the DFT calculation when the vibration-induced dipole moment direction is taken into consideration. For dipole moments along the  $a$ -direction, DFT calculation predicts vibrational modes at 2.76, 3.16, 3.33, and 4.28 THz. Additional modes are calculated at 5.46 and 6.33 THz, beyond the experimental frequency

TABLE I: Observed absorption bands positions along each crystallographic axis compared to the closest DFT calculated mode position. Modes are designated by frequency (in THz) with experimental modes at 10 K.

Here,  $\parallel$  denotes being parallel with respect to the incident electric field of the polarized light.

$\vec{E} \parallel a$ -axis		$\vec{E} \parallel b$ -axis		$\vec{E} \parallel c$ -axis	
Experiment	DFT	Experiment	DFT	Experiment	DFT
2.74	2.76	2.25	2.18	2.94	2.84
3.12	3.16	2.63	2.65	3.34	3.58
3.26	3.33	3.30	3.41	3.79	3.85
4.25	4.28	4.71	4.68	4.31	4.25
	5.46		4.96	5.08	4.93
	6.33		6.51	6.44	
				7.08	7.11

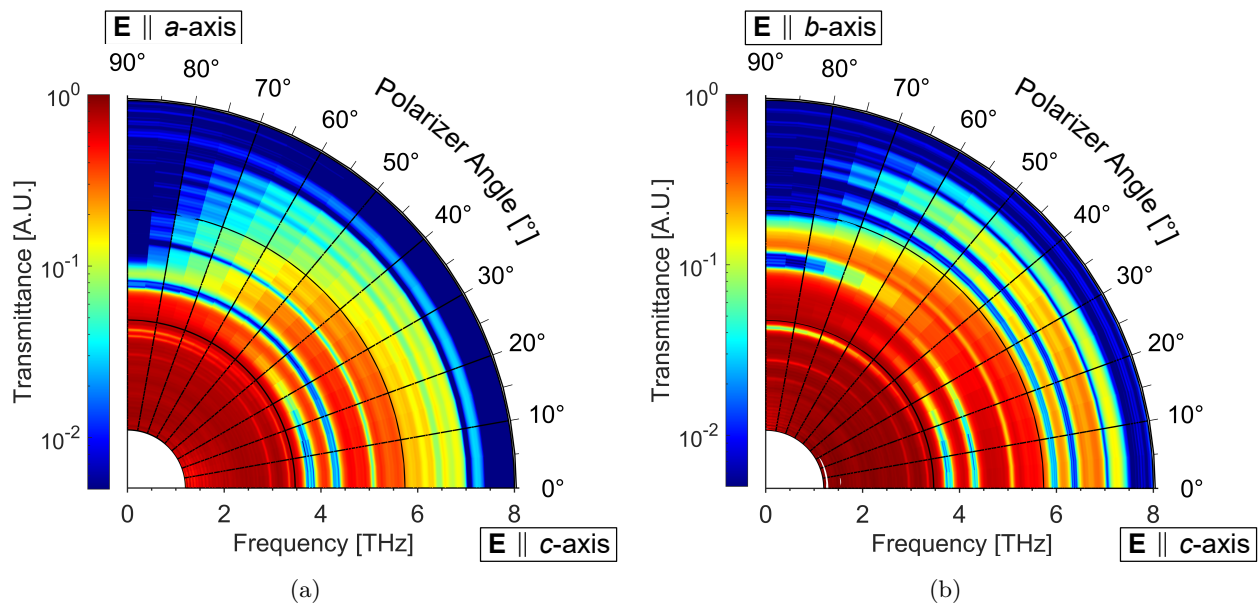


FIG. 3: Polarized THz measurements at 7K as the direction of  $\vec{E}$  is varied. (a)  $a$ -axis to  $c$ -axis. (b)  $b$ -axis to  $c$ -axis.

cutoff of approximately 4.5 THz.

In the  $b$ -direction, absorption bands are observed at 2.25, 2.63, and 3.30 THz. A broad absorption appears at 4.71 THz and is absorptive enough to reach the noise floor. The observations agree with the DFT calculations of modes at 2.18, 2.65, 3.41, and 4.68 THz. A further mode is calculated at 4.96 THz. While not associable with an additional unique experimental absorption beyond that at 4.71 THz, it may be merged with the 4.71 THz absorption, given it is broad and it is incompletely resolved. An additional calculated mode at 6.51 THz lies above the cutoff frequency of the  $b$ -axis polarization at 5.70 THz.

The  $c$ -direction polarization shows absorption bands at 2.94, 3.34, 3.79, 4.31, 5.08, 6.44, and 7.08 THz. DFT calculates modes at 2.84, 3.58, 3.85, 4.25, 4.93, and 7.11 THz. These are all in good agreement with the experimental absorptions, with the exception of the observed absorption at 6.44 THz. However, this feature does not have the same Lorentzian-like profile as the rest of the absorption bands assigned, and could reasonably be a non-resonant feature in origin. The frequency cutoff along the  $c$ -axis is approximately 7.5 THz.

Previous work using unpolarized light [37] assigns the same DFT modes. However, it does so to different experimental modes in five cases, namely the 3.41, 3.58, 4.24, 4.28, and 4.96 THz modes. This clearly shows the improved reliability of studies using polarized spectra. An additional DFT mode at 7.11 THz is identified here which was not presented in the earlier work.

As mentioned above, the polarization data exhibits frequency cutoffs of approximately 4.5 THz for the  $a$ -axis, 5.7 THz for the  $b$ -axis, and 7.5 THz for the  $c$ -axis, which

is the same for the anisotropic spectra. These results are consistent with and extend a previous report on the reflection THz spectrum of L-alanine [23] which shows strong, broad reflection beyond 4.8 THz perpendicular to the  $c$ -axis, but no significant broad, intense reflections parallel to the  $c$ -axis. Thus, it is not absorption, but rather strong reflection which most likely affects the frequency cutoff in the  $a$ - and  $b$ -directions.

In summary, our DFT modeling of dipoles excited along specific crystal directions agrees very well with our experimental polarization results. This lends confidence to the physical basis of the DFT calculations. Specifically, the success of the B97-3c functional in providing very accurate mode calculations has verified that weak hydrogen and van der Waals bonds are critical to the origin of the fundamental modes of L-alanine. Experimentally, through the use of polarized THz spectroscopy, closely-spaced absorption bands have been now separated, confirming an additional mode at 3.30 THz (with a dipole moment along the  $b$ -axis). Comparison with the DFT modelling has also extended the assignment of modes made in previous work [37]. Anisotropic theory combined with polarized experiments thus resolves the fundamental modes of L-alanine.

This research used the THz/Far-IR beamline at the Australian Synchrotron, part of ANSTO, the Australian Nuclear Science and Technology Organisation. We thank D. Appadoo and R. Plathe for assistance. Numerical modeling was assisted by the National Computational Infrastructure (NCI), supported by the Australian Government. We thank AINSE Ltd for financial assistance (Award-PGRA) to enable this research, also supported by Australian Research Council DP160101474.

- 
- \* ja846@uowmail.edu.au
- [1] M. S. Lehmann, T. F. Koetzle, and W. C. Hamilton, *Journal of the American Chemical Society* **94**, 2657 (1972).
  - [2] P. G. Higgs and R. E. Pudritz, *Astrobiology* **9**, 483 (2009).
  - [3] V. Kubyshkin and N. Budisa, *International Journal of Molecular Sciences* **20** (2019).
  - [4] S. Ioppolo, G. Fedoseev, K. Chuang, H. Cuppen, A. Clements, M. Jin, R. Garrod, D. Qasim, V. Kofman, E. van Dishoeck, and H. Linnartz, *Nature Astronomy* **5**, 197 (2021).
  - [5] T. Chen, Z. Li, and W. Mo, *Spectrochimica Acta Part A: Molecular and Biomolecular Spectroscopy* **106**, 48 (2013).
  - [6] T. Kleine-Ostmann, R. Wilk, F. Rutz, M. Koch, H. Niemann, B. Güttler, K. Brandhorst, and J. Grunenberg, *ChemPhysChem* **9**, 544 (2008).
  - [7] S. C. Shen, L. Santo, and L. Genzel, *International Journal of Infrared & Millimeter Waves* **28**, 595 (2007).
  - [8] M. R. C. Williams, A. B. True, A. F. Izmaylov, T. A. French, K. Schroeck, and C. A. Schmuttenmaer, *Physical Chemistry Chemical Physics* **13**, 11719 (2011).
  - [9] W. Yi, J. Yu, Y. Xu, F. Wang, Q. Yu, H. Sun, L. Xu, Y. Liu, and L. Jiang, *Instrumentation Science & Technology* **45**, 423 (2017).
  - [10] W.-N. Wang, H.-Q. Li, Y. Zhang, and C.-L. Zhang, *Acta Physico-Chimica Sinica* **25**, 2074 (2009).
  - [11] L. M. Lepodise, *Spectrochimica Acta Part A: Molecular and Biomolecular Spectroscopy* **217**, 35 (2019).
  - [12] L. Xie, C. Wang, M. Chen, B.-B. Jin, R. Zhou, Y. Huang, S. Hameed, and Y. Ying, *Spectrochimica Acta Part A: Molecular and Biomolecular Spectroscopy* **222**, 117179 (2019).
  - [13] Y. He, P. I. Ku, J. R. Knab, J. Y. Chen, and A. G. Markelz, *Physical Review Letters* **101**, 178103 (2008).
  - [14] M. Hutereau, P. A. Banks, B. Slater, J. A. Zeitler, A. D. Bond, and M. T. Ruggiero, *Physical Review Letters* **125**, 103001 (2020).
  - [15] R. A. Lewis, *Terahertz Physics* (Cambridge University Press, Cambridge, UK, 2013).
  - [16] S. S. Dhillon, M. S. Vitiello, E. H. Linfield, A. G. Davies, M. C. Hoffmann, J. Booske, C. Paoloni, M. Gensch, P. Weightman, G. P. Williams, E. Castro-Camus, D. R. S. Cumming, F. Simoens, I. Escorcia-Carranza, J. Grant, S. Lucyszyn, M. Kuwata-Gonokami, K. Konishi, M. Koch, C. A. Schmuttenmaer, T. L. Cocker, R. Huber, A. G. Markelz, Z. D. Taylor, V. P. Wallace, J. A. Zeitler, J. Sibik, T. M. Korter, B. Ellison, S. Rea, P. Goldsmith, K. B. Cooper, R. Appleby, D. Pardo, P. G. Huggard, V. Krozer, H. Shams, M. Fice, C. Renaud, A. Seeds, A. Stöhr, M. Naftaly, N. Ridler, R. Clarke, J. E. Cunningham, and M. B. Johnston, *Journal of Physics D: Applied Physics* **50**, 043001 (2017).
  - [17] J. Liu, K. Dona, G. Hoshino, S. Knirck, N. Kurinsky, M. Malaker, D. W. Miller, A. Sonnenschein, M. H. Awida, P. S. Barry, K. K. Berggren, D. Bowring, G. Carosi, C. Chang, A. Chou, R. Khatiwada, S. Lewis, J. Li, S. W. Nam, O. Noroozian, and T. X. Zhou (BREAD Collaboration), *Phys. Rev. Lett.* **128**, 131801 (2022).
  - [18] J. He, X. He, T. Dong, S. Wang, M. Fu, and Y. Zhang, *Journal of Physics D: Applied Physics* **55**, 123002 (2021).
  - [19] X. Li, T. Qiu, J. Zhang, E. Baldini, J. Lu, A. M. Rappe, and K. A. Nelson, *Science* **364**, 1079 (2019).
  - [20] H. Hoshina, Y. Morisawa, H. Sato, H. Minamide, I. Noda, Y. Ozaki, and C. Otani, *Physical Chemistry Chemical Physics* **13**, 9173 (2011).
  - [21] Y. Deng, J. A. McKinney, D. K. George, K. A. Niessen, A. Sharma, and A. G. Markelz, *ACS Photonics* **8**, 658 (2021).
  - [22] R. Singh, D. K. George, J. B. Benedict, T. M. Korter, and A. G. Markelz, *The Journal of Physical Chemistry A* **116**, 10359 (2012).
  - [23] Z. Mita, H. Watanabe, and S. Kimura, *Infrared Physics & Technology* **96**, 7 (2019).
  - [24] N. Laman, S. Harsha, D. Grischkowsky, and J. S. Melinger, *Biophysical Journal* **94**, 1010 (2008).
  - [25] Y. Liu, T. Zhou, and J.-C. Cao, *Infrared Physics & Technology* **96**, 17 (2019).
  - [26] J. Darkwah, G. Smith, I. Ermolina, and M. Mueller-Holtz, *International Journal of Pharmaceutics* **455**, 357 (2013).
  - [27] C. Ponceca, O. Kambara, S. Kawaguchi, K. Yamamoto, and K. Tominaga, *Journal of Infrared, Millimeter, and Terahertz Waves* **31**, 799 (2010).
  - [28] A. R. Taulbee, J. A. Heuser, W. U. Spindel, and G. E. Pacey, *Analytical Chemistry* **81**, 2664 (2009).
  - [29] J. Nishizawa, T. Sasaki, K. Suto, T. Tanabe, T. Yoshida, T. Kimura, and K. Saito, *International Journal of Infrared and Millimeter Waves* **27**, 779 (2006).
  - [30] A. Matei, N. Drichko, B. Gompf, and M. Dressel, *Chemical Physics* **316**, 61 (2005).
  - [31] M. Yamaguchi, F. Miyamaru, K. Yamamoto, M. Tani, and M. Hangyo, *Applied Physics Letters* **86**, 053903 (2005).
  - [32] M. Barthes, A. F. Vik, A. Spire, H. N. Bordallo, and J. Eckert, *The Journal of Physical Chemistry A* **106**, 5230 (2002).
  - [33] L. Jiang, J. Yu, C. Li, W. Yi, Y. Xu, and Y. Liu, in *2016 41st International Conference on Infrared, Millimeter, and Terahertz waves (IRMMW-THz)* (2016) pp. 1–2.
  - [34] W. Guo and W. Wei-Ning, *Acta Physico-Chimica Sinica* **28**, 1579 (2012).
  - [35] Z.-P. Zheng and W. Fan, *Journal of Biological Physics* **38**, 405 (2012).
  - [36] F. Zhang, H.-W. Wang, K. Tominaga, and M. Hayashi, *The Journal of Physical Chemistry A* **119**, 3008 (2015).
  - [37] T. J. Sanders, J. L. Allen, J. Horvat, and R. A. Lewis, *The Journal of Chemical Physics* **154**, 244311 (2021).
  - [38] See Supplemental Material at [link], for details about the calculations and instrumentation, comparison of  $c$ -axis spectra, triple-axis neutron scattering for the 120 reflection, and a comparison to the unpolarized spectrum.
  - [39] R. Dovesi, A. Erba, R. Orlando, C. M. Zicovich-Wilson, B. Civalleri, L. Maschio, M. Rérat, S. Casassa, J. Baima, S. Salustro, and B. Kirtman, *WIREs Computational Molecular Science* **8**, e1360 (2018).
  - [40] J. G. Brandenburg, C. Bannwarth, A. Hansen, and S. Grimme, *The Journal of Chemical Physics* **148**, 064104 (2018).
  - [41] S. Grimme, J. Antony, S. Ehrlich, and H. Krieg, *The Journal of Chemical Physics* **132**, 154104 (2010).
  - [42] S. A. Katsyuba, E. E. Zvereva, and S. Grimme, *The Journal of Physical Chemistry A* **123**, 3802 (2019).
  - [43] F. Weigend and R. Ahlrichs, *Physical Chemistry Chem-*

- ical Physics **7**, 3297 (2005).
- [44] S. Grimme, J. G. Brandenburg, C. Bannwarth, and A. Hansen, *The Journal of Chemical Physics* **143**, 054107 (2015).
- [45] P. R. Tulip and S. J. Clark, *The Journal of Chemical Physics* **121**, 5201 (2004).
- [46] F. Pascale, C. M. Zicovich-Wilson, F. López Gejo, B. Civalleri, R. Orlando, and R. Dovesi, *Journal of Computational Chemistry* **25**, 888 (2004).
- [47] C. M. Zicovich-Wilson, F. Pascale, C. Roetti, V. R. Saunders, R. Orlando, and R. Dovesi, *Journal of Computational Chemistry* **25**, 1873 (2004).
- [48] T. P. Srinivasan, R. Indirajith, and R. Gopalakrishnan, *Journal of Crystal Growth* **318**, 762 (2011).
- [49] S. A. Danilkin and M. Yethiraj, *Neutron News* **20**, 37 (2009).
- [50] F. Massimino, M. Bruno, M. Rubbo, and D. Aquilano, *Crystal Research and Technology* **46**, 789 (2011).

# Combining Density-Functional Theory with Low-Temperature, Polarized Terahertz Spectroscopy of Single Crystals Explicates the Fundamental Modes of L-Alanine SUPPLEMENTAL

J. L. Allen, T. J. Sanders, J. Horvat, and R. A. Lewis  
*Institute for Superconducting and Electronic Materials and School of Physics,  
University of Wollongong, Wollongong, NSW 2522, Australia.\**

K. C. Rule  
*Australian Centre for Neutron Scattering, Australian Nuclear Science  
and Technology Organisation, Lucas Heights, NSW 2234, Australia*  
(Dated: November 30, 2022)

## I. FURTHER THEORETICAL CONSIDERATIONS

### A. Finer details of the DFT calculation

The energy convergence tolerance, in self-consistent field cycles, was  $7 \times 10^{-14}$  hartree/atom ( $2 \times 10^{-12}$  eV/atom). The geometrical convergence criteria were: maximum energy gradient  $4 \times 10^{-6}$  hartree/bohr ( $2 \times 10^{-4}$  eV/Å), RMS energy gradient  $< 10^{-6}$  hartree/bohr ( $5 \times 10^{-5}$  eV/Å), maximum atomic displacement  $10^{-5}$  bohr and RMS displacement  $4 \times 10^{-6}$  bohr. A Monkhorst-Pack grid of  $13 \times 13 \times 13$  was used to ensure this high level of convergence. Full geometry optimization was performed, including both atomic positions within the unit cell, as well as the unit cell parameters. The fully converged geometry resulted in a band gap of 5.12 eV. This is 8% above the experimental band gap of 4.75 eV [1].

### B. Anharmonicity

In all DFT computational packages, the normal mode analysis is performed in the harmonic approximation. In effect, the calculations assume absolute zero of thermodynamic temperature; thermally-induced non-linearities are ignored. We designed our experiment to match this assumption, by measuring at low temperatures.

At non-zero temperatures, anharmonic effects come into play. These may be monitored by tracking the change of frequency of the mode with temperature. Generally speaking, the modes decrease in energy (or “red-shift”) as temperature increases. We have previously observed this phenomena for L-alanine [2] as well as for DL-alanine [3], and for other amino acids, including L-phenylalanine [4],  $\alpha$ -glycine [5], and L-tyrosine [6]. The change in frequency with temperature is well-accounted for within a Bose-Einstein model.

In principle, it may be possible to calculate the true potential along the vector of each normal mode and check by how much each mode deviates from the harmonic potential as a function of temperature. However, this is beyond the scope of the present work, where the main focus is on polarization. That is, we calculate the direction of the change of dipolar moment obtained by the modeling in the harmonic approximation and compare this directly with the measurements taken using light polarized along specific crystal axes at low temperature.

---

\* ja846@uowmail.edu.au

## II. THZ INSTRUMENTATION

Unpolarized temperature-dependent spectra have been measured on a Fourier transform spectrometer (FTS) to observe modes in the range 1–8 THz ( $30\text{--}250\text{ cm}^{-1}$ ) (see Fig. S1). A broadband coated mylar beamsplitter was used to measure these spectra at an instrumental resolution of  $0.015\text{ THz}$  ( $0.5\text{ cm}^{-1}$ ) without apodization. The Bomem DA8 FTS system was used in conjunction with a THz semiconductor bolometer as the detector. A sample temperature range of 12–300 K was made accessible via a liquid-helium continuous-flow cryostat (Oxford Instruments OptistatCF) with an outer vacuum which was evacuated to approximately  $10^{-5}\text{ mBar}$ . The instrumental uncertainty for the temperature was  $\pm 0.1\text{ K}$ . Cryostat windows used were polyethylene.

The absorption bands observed in Fig. S1 show temperature-dependent frequency shifting. This indicates that the absorption bands correspond to vibrational modes, which are expected to undergo thermal shifting [5].

Polarization measurements were carried out on a separate FTS system (Bruker IFS125) with the Australian Synchrotron being used as a bright THz radiation source. A  $6\text{-}\mu\text{m}$  multi-layer mylar beamsplitter was used with a 4.2 K silicon bolometer, also at an unapodized resolution of  $0.015\text{ THz}$ . A polyethylene (wire) grid polarizer was used to polarize the synchrotron THz radiation incident on the samples.

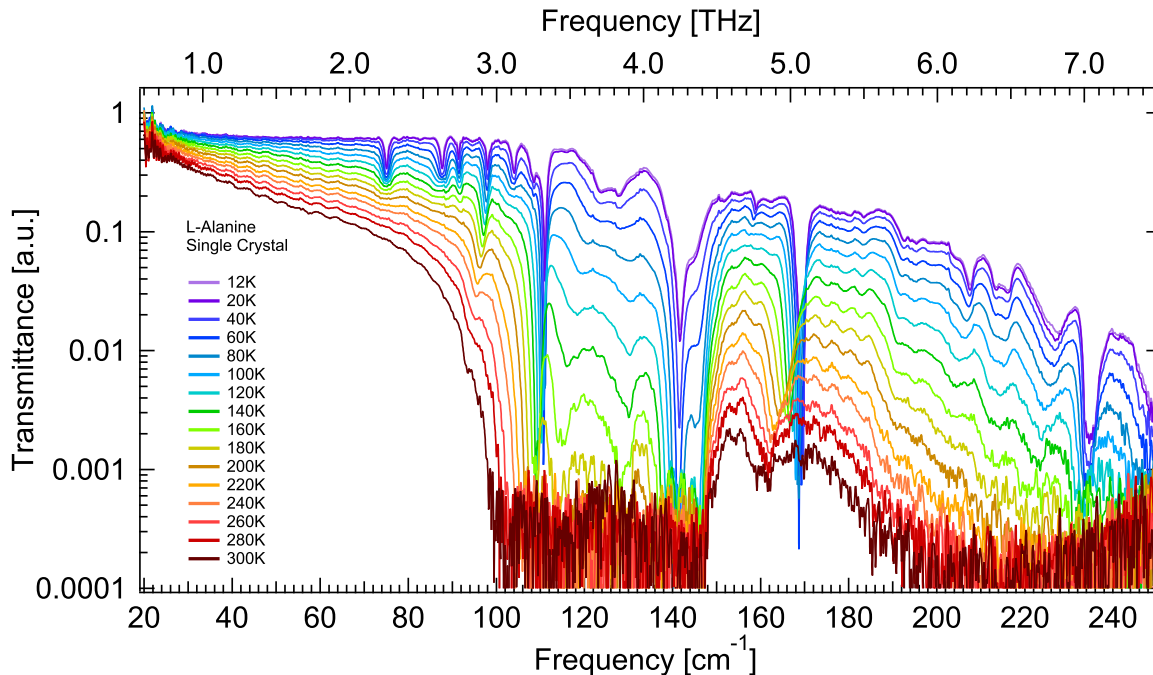


Fig. S1: Single-crystal L-alanine spectra measured at temperatures between 12 K and 300 K. Reproduced from Ref. [2].



### III. COMPARISON OF C-AXIS SPECTRA

Spectra for polarization along the  $c$ -axis were measured using two different crystals, since the  $c$ -axis was the mutual axis for the two crystals used; one was sanded to be in the  $a$ - $c$ -plane and one in the  $b$ - $c$ -plane. Fig. S2 shows the comparison of the  $c$ -axis spectra for these two crystals.

The crystal with  $b$ - $c$ -plane geometry shows absorption bands at 5.85 THz and 6.33 THz, where the alternate crystal in the  $a$ - $c$ -plane geometry does not. One may postulate that the origin of these features could be contaminants, since they only appear in one sample. However, a more likely explanation is as components of the  $a$ -axis modes. While known  $a$ -axis vibrational modes are not seen at lower frequencies, it is usual that higher-frequency absorptions are stronger. So a small component of an axis other than the  $c$ -axis could have a strong effect at large frequencies. There are DFT calculated modes in the  $a$ -axis at 5.43 THz and 6.30 THz. There is only one mode calculated in  $b$ -axis in this region, at 6.51 THz. Thus, these modes can also be reasonably assigned to those calculated in the  $a$ -axis.

The rest of the spectra for the  $c$ -axis for each crystal is highly reproducible, which is commensurate with pure samples.

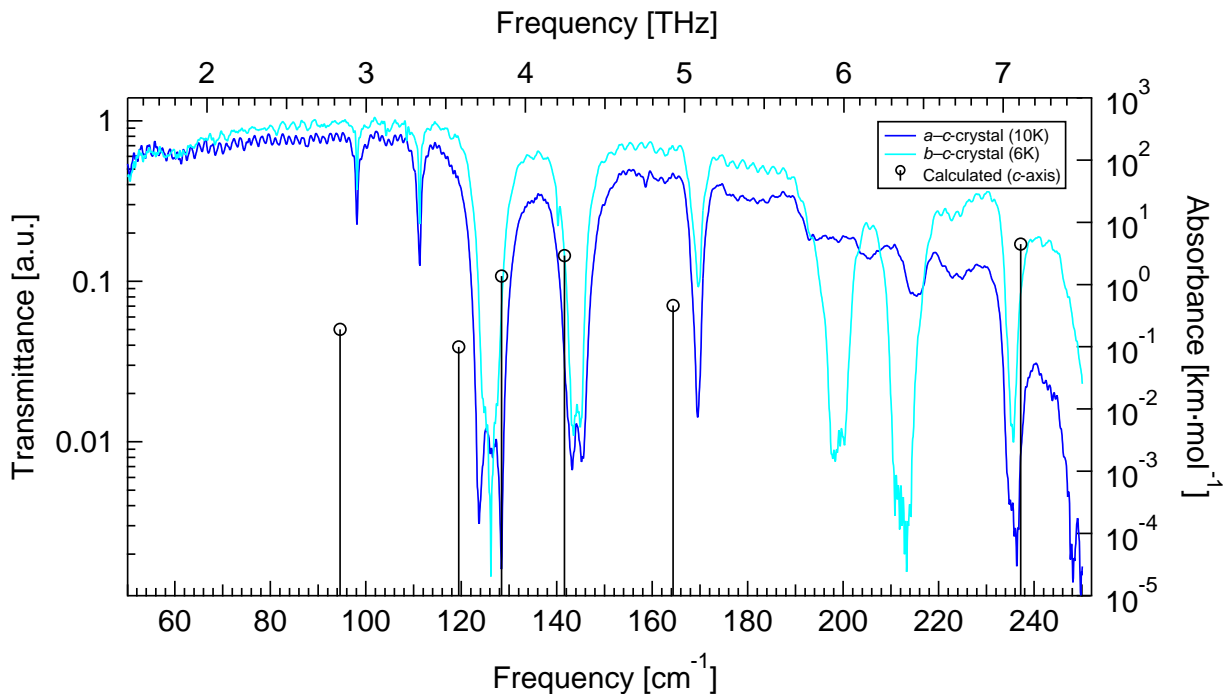


Fig. S2: Polarized THz measurements at 10 K along the crystallographic  $c$ -axis of L-alanine for both crystals measured. Additional modes appear for the crystal with the  $c$ - $b$ -axes in the normal plane.

#### IV. TRIPLE-AXIS NEUTRON SCATTERING

The 120 and 040 reflections were measured for the L-alanine single crystal grown with the normal face in the  $a$ - $c$ -plane. Figure S3 shows a narrow mosaic spread of  $\sim 0.8^\circ$  for the 120 reflection which has been fitted with a Gaussian. Additionally, reciprocal space scans show only 0.06 reciprocal lattice units as the peak full width at half maximum (FWHM). This indicates highly ordered single-crystallinity without any twinning effects.

Neutron scattering probes the entire bulk of a sample, since uncharged neutrons interact only with the nuclei of atoms and penetrate into the bulk. This corresponds well with the THz spectroscopy measurements which also probe the bulk of the sample.

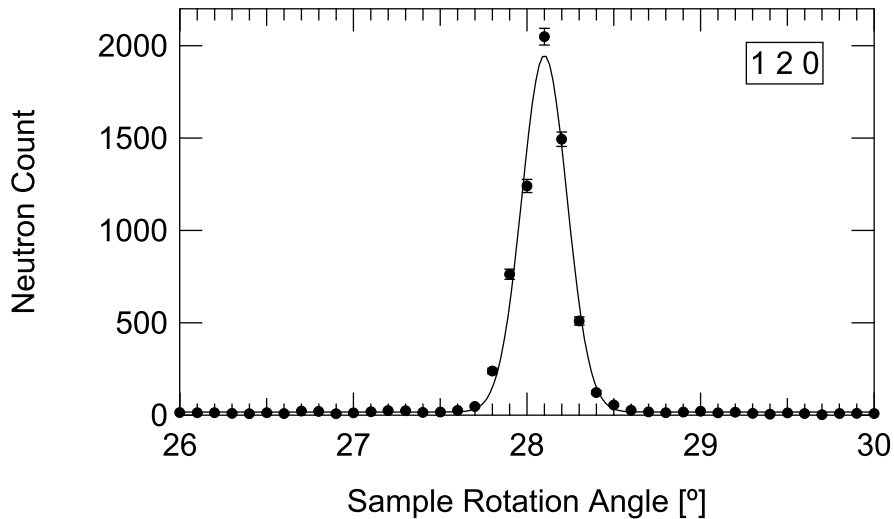


Fig. S3: The 120 reflection of a single crystal of L-alanine measured with 2.345 Å neutrons at ANSTO using the Taipan thermal triple-axis spectrometer. The abscissa refers to the rotation angle of the sample about its center axis.

## V. COMPARISON TO UNPOLARIZED SPECTRUM

For ease of comparison, Fig. S4 displays together the unpolarized spectrum and the spectra for light polarized along each of the three principal crystallographic axes. We make three observations concerning these.

First, it is clear that the absorption bands in the unpolarized spectrum are all reproduced in one of the polarized spectra. The anisotropic technique of polarizing the incident beam successively along each of the three principal axes of the crystal thus effectively works to separate out the vibrational modes associated with electric dipole moments directly along each crystallographic direction.

Secondly, the unpolarized spectrum has no significant contributions from the *a*- nor the *b*-axes above approximately 5.1 THz, since all the light along these directions has been absorbed in this region. Thus, only the features corresponding to the *c*-axis contributes to the spectrum in this region. The features seen from 5.7 THz to 6.9 THz in the unpolarized spectrum are the non-resonant features associated with the *c*-axis.

Thirdly, the inset of Fig. S4 shows the region from around 3.3 THz. The unpolarized spectrum in this region has only two absorption peaks, at 3.26 THz and 3.34 THz. These correspond to absorptions in the *a*- and *c*-directions, respectively. However, an extra mode is revealed along the *b*-axis at 3.30 THz. This is obscured in the unpolarized spectrum and has been revealed through the polarized measurements. This extends the mode assignment possible with polarized THz spectroscopy.

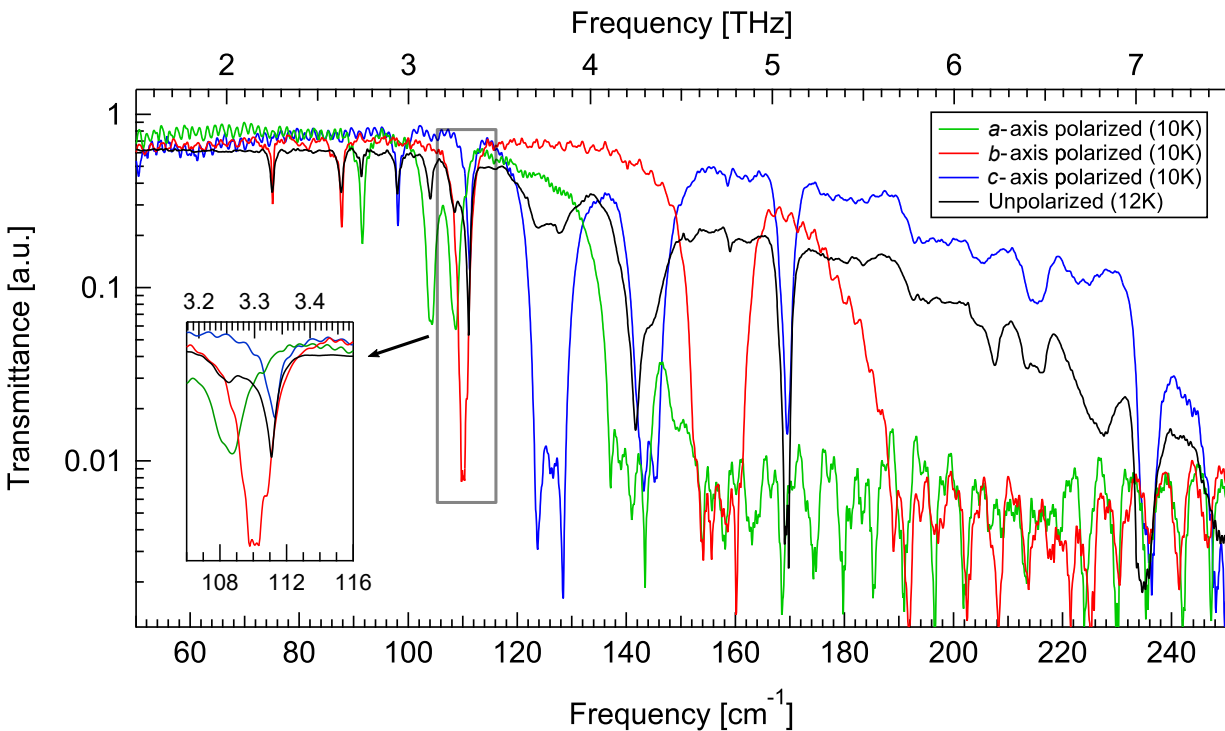


Fig. S4: Comparison of the polarized spectra with the unpolarized spectrum of single-crystalline L-alanine. The inset shows the details at around 3.3 THz where three vibrational modes overlap. In the unpolarized spectrum, only two peaks are distinguishable.

- 
- [1] F. Akhtar and J. Podder, *Research Journal of Physics* **6**, 31 (2012).
  - [2] T. J. Sanders, J. L. Allen, J. Horvat, and R. A. Lewis, *The Journal of Chemical Physics* **154**, 244311 (2021).
  - [3] T. J. Sanders, J. L. Allen, J. Horvat, and R. A. Lewis, *Phys. Chem. Chem. Phys.* **23**, 657 (2021).
  - [4] J. L. Allen, T. J. Sanders, R. Plathe, D. Appadoo, J. Horvat, and R. A. Lewis, *Spectrochimica Acta Part A: Molecular and Biomolecular Spectroscopy* **260**, 119922 (2021).
  - [5] J. L. Allen, T. J. Sanders, J. Horvat, and R. A. Lewis, *Spectrochimica Acta Part A: Molecular and Biomolecular Spectroscopy* **244**, 118635 (2021).
  - [6] T. J. Sanders, J. L. Allen, R. Plathe, D. Appadoo, J. Horvat, and R. A. Lewis, *Spectrochimica Acta Part A: Molecular and Biomolecular Spectroscopy* **286**, 121970 (2023).